RADIATIVE RETURN CAPABILITIES OF A HIGH-ENERGY, HIGH-LUMINOSITY e^+e^- COLLIDER

Marek Karliner^{a†}. Matthew Low^{b,c‡}, Jonathan L. Rosner^{b§}, and Lian-Tao Wang^{b,c¶}

^{a} *School of Physics and Astronomy*
Raymond and Beverly Sackler Faculty of Exact Sciences
Tel Aviv University, Tel Aviv 69978, Israel

^{b} *Enrico Fermi Institute and Department of Physics*
University of Chicago, 5620 S. Ellis Avenue, Chicago, IL 60637, USA

^{c} *Kavli Institute for Cosmological Physics*
University of Chicago, 933 E. 56th Street, Chicago, IL 60637, USA

ABSTRACT

An electron-positron collider operating at a center-of-mass energy E_{CM} can collect events at all lower energies through initial-state radiation (ISR or *radiative return*). We explore the capabilities for radiative return studies by a proposed high-luminosity collider at $E_{CM} = 250$ or 90 GeV, to fill in gaps left by lower-energy colliders such as PEP, PETRA, TRISTAN, and LEP. These capabilities are compared with those of the lower-energy e^+e^- colliders as well as hadron colliders such as the Tevatron and the CERN Large Hadron Collider (LHC). Some examples of accessible questions in dark photon searches and heavy flavor spectroscopy are given.

PACS codes: 13.66.Bc, 13.66.De, 13.66.Hk

I   Introduction

An electron-positron collider operating at a center-of-mass energy E_{CM} can collect events at all lower energies through initial-state radiation (ISR). This *radiative return* process has been used to good advantage in e^+e^- colliders such as DAΦNE, PEP-II, KEK-B, and LEP [1–4]. In the present paper we explore the capabilities of a higher-energy high-luminosity e^+e^- collider such as that envisioned by CERN (FCC-ee) [5] or China (CEPC) [6], operating at $E_{CM} \simeq 250$ or 90 GeV (functioning as a Giga- or Tera-Z factory at the latter energy) [7], to perform radiative return studies of physics at lower center-of-mass energies.

In order to fairly assess the capabilities of future colliders with past and present colliders it is necessary to specify the total integrated luminosity expected to be collected by future

†`marek@proton.tau.ac.il`
‡`mattlow@uchicago.edu`
§`rosner@hep.uchicago.edu`
¶`liantaow@uchicago.edu`

Table I: Projected luminosities for the CEPC [8] and FCC-ee [9]. These values are used throughout the text.

	$\sqrt{s} = 90$ GeV	$\sqrt{s} = 250$ GeV
CEPC	0.5 ab^{-1}	5 ab^{-1}
FCC-ee	50 ab^{-1}	10 ab^{-1}

colliders. Based on current design reports, over 2 interaction points the CEPC is expected to collect 500 fb^{-1} on the Z pole, which corresponds to approximately 1×10^{10} Z's, and 5 ab^{-1} at $E_{CM} \simeq 250$ GeV [8]. The FCC-ee, over 4 interaction points, is expected to collect 50 ab^{-1}, which is roughly 1×10^{12} Z's, at $E_{CM} \simeq 90$ GeV and 10 ab^{-1} at $E_{CM} \simeq 250$ GeV [9]. Table I summarizes these numbers. For convenience where the exact number of events is not imporant, we shall occasionally quote results for a nominal integrated luminosity of 1 ab^{-1}. These values may be rescaled appropriately.

We briefly review some previous uses of radiative return in Section II. In Section III we study narrow resonance production, while the discussion is extended to continuum production in Section IV. Section V compares the reach of e^+e^- and hadron colliders for two benchmark processes: "dark photon" and $b\bar{b}$ production. Some processes of interest in heavy flavor spectroscopy are noted in Section VI. We conclude in Section VII. Some calculational checks are contained in two Appendices: VIII and IX.

II   Some previous uses of radiative return

Considerable use has been made of radiative return in previous experiments using electron-positron colliders. In Table II we summarize some parameters of experiments at these colliders [11,12]. Maximum instantaneous luminosities of circular e^+e^- colliders are plotted versus year in Fig. 1.

A   KLOE at DAΦNE

The DAΦNE accelerator at Frascati operates near or at the CM energy (1020 MeV) of the ϕ resonance. It has studied the cross section $e^+e^- \to \pi^+\pi^-$ at lower CM energies via the process $e^+e^- \to \gamma\pi^+\pi^-$, where the photon is emitted in initial-state radiation, with the main purpose of reducing the error in the hadronic vacuum polarization contribution to the anomalous magnetic moment a_μ of the muon. Three sets of data are reported: 141.4 pb^{-1} studying the interval $0.35 < M_{\pi\pi}^2 < 0.95$ GeV^2 [14], 240 pb^{-1} studying the same interval [15, 16], and 230 pb^{-1} studying $0.1 < M_{\pi\pi}^2 < 0.85$ GeV^2 [17]. KLOE also has searched for "dark photons" below 1 GeV decaying to e^+e^- and $\mu^+\mu^-$, as noted in more detail later [18, 19].

B   CLEO at CESR

The CLEO Collaboration used initial-state radiation to search for the state $X(3872)$ [20] in e^+e^- collisions at the Cornell Electron Storage Ring (CESR). The absence of a signal

Table II: Instantaneous and/or integrated luminosities achieved at some e^+e^- colliders. Based in part on Section 30 of Ref. [11], with values from Ref. [12] for PETRA, PEP, and TRISTAN. We thank G. Alexander and S. L. Wu for help with some of these estimates.

Collider	Detector	CM energy (GeV)	Max. $\mathcal{L}$ (10^{30} cm^{-2}s^{-1})	$\int \mathcal{L} dt$ (fb^{-1})
DAΦNE	KLOE	1.02	453	2.5
		1.00	453	0.23
CESR	CLEO	9.46–11.30	1280 at 10.6 GeV	15.1
PEP-II	BaBar	10.58	12069	424.7
		10.18	. . .	43.9
KEK-B	Belle	9.46–10.89	21083	980
PEP		29	60	1.167[a]
PETRA		46.8[b]	24 at 35 GeV	0.817[c]
TRISTAN		64[b]	40	0.942[d]
LEP		M_Z	24	0.808[e]
		> 130	34–90	2.980[e]

[a] Summed over detectors DELCO, HRS, MAC, Mark II, TPC/2γ

[b] Maximum value

[c] Summed over detectors CELLO, JADE, Mark J, PLUTO, TASSO

[d] Summed over detectors AMY, TOPAZ, VENUS

[e] Summed over detectors ALEPH, DELPHI, L3, OPAL

served as partial evidence that the state did not have spin 1 and negative parity and charge-conjugation eigenvalue.

C   BaBar at PEP-II

The initial-state radiation process has been used to great advantage by the BaBar Collaboration at PEP-II. Just in the past three years, papers have appeared on the production of $\pi^+\pi^-\pi^+\pi^-$ [21]; $K^+K^-\pi^+\pi^-$, $K^+K^-\pi^0\pi^0$, $K^+K^-\pi^+\pi^-$ [22]; $\pi^+\pi^-$ [23]; $J/\psi\pi^+\pi^-$ [24]; $p\bar{p}$ [25]; K^+K^- [26]; $\psi(2S)\pi^+\pi^-$ [27]; and a variety of final states with two neutral kaons [28]. The CM energies and integrated luminosities in Table II are those quoted for BaBar in the last paper. The final states involving light hadrons contribute to reducing the uncertainty on the hadronic vacuum polarization contribution to a_μ and to the running of the fine structure constant in precision electroweak studies, while those involving J/ψ and $\psi(2S)$ are of interest for resonant structures.

D   Belle at KEK-B

Since 2011 the Belle Collaboration has produced a couple of initial-state radiation studies, involving production of $J/\psi K^+K^-$ and $J/\psi K_S K_S$ [29]; and $\psi(2S)\pi^+\pi^-$ [30]. The focus of this work has been the search for resonant substructures in the final states.
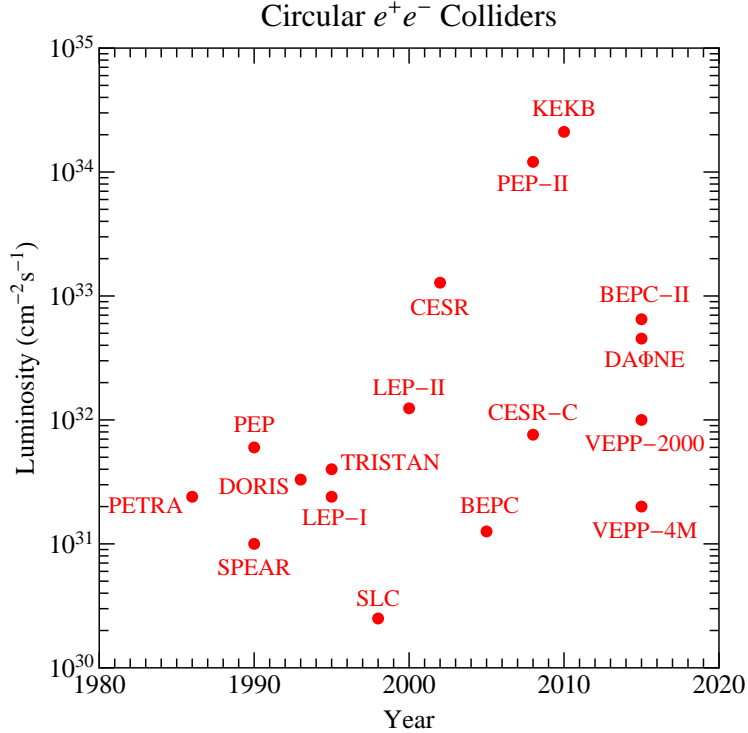
Figure 1: Maximum instantaneous luminosities of circular e^+e^- colliders versus time. Adapted from Fig. 1 of Ref. [13].

E   LEP Collaborations

The LEP entries in Table II refer to total integrated luminosities at various energies. Results from specific detectors are not always based on these totals, as many of them were obtained before the full data sample was available.

E.1   ALEPH

The reaction $e^+e^- \to \gamma_{\text{ISR}}\,\mu^+\mu^-$ has been used by the ALEPH Collaboration [31] to study the cross section and forward-backward asymmetry for $e^+e^- \to \mu^+\mu^-$ in the CM energy range 20–136 GeV.

E.2   DELPHI

The helicity structure in $e^+e^- \to \mu^+\mu^-$ is particularly sensitive to new physics in the CM energy range around 80 GeV, which is accessible through the process $e^+e^- \to \gamma_{\text{ISR}}\mu^+\mu^-$ The DELPHI Collaboration [32] has studied this process, finding no evidence for new physics.

E.3   L3

The L3 Collaboration has used ISR to measure muon pair production in e^+e^- collisions between 50 and 86 GeV [33]. This study was motivated in part by the need to fill a gap between the maximum energy of the TRISTAN accelerator at KEK (about 62 GeV) and the mass of the Z.

E.4 OPAL

The OPAL Collaboration pioneered the use of ISR at LEP to fill the aforementioned gap between 62 GeV and M_Z [34]. No deviations from the standard model were found, albeit with a very early data sample. The collaboration used radiative fermion pair events to perform a LEP beam energy measurement [35]. Fig. 1 of this reference gives an idea of the yield that may be expected from radiative return studies with beam energies approaching 200 GeV. An extensive study was made, accumulating a total of 1.132 fb^{-1} at LEP CM energies between 183 and 207 GeV. Aside from a copious Z peak, the numbers of events per 2 GeV subenergy at a subenergy of 125 GeV were about 200 for $q\bar{q}$, a dozen for $\mu^+\mu^-$, and three dozen for $\tau^+\tau^-$. Supposing one had a sample of 1 ab^{-1} at $E_{CM} = 250$ GeV, one might expect $\mathcal{O}(2 \times 10^5)$ hadronic events, $\mathcal{O}(10^4)$ $\mu^+\mu^-$ events, and a few tens of thousand $\tau^+\tau^-$ events, per 2 GeV bin in invariant mass around 125 GeV.

III   Resonance production

The cross section for electron-positron production of a vector meson resonance R with mass m_R and e^+e^- partial width Γ_{ee} decaying to a final state f with partial width Γ_f may be written near resonance as

$$\sigma(e^+e^- \to R \to f;\ s) = \frac{12\pi\Gamma_{ee}\Gamma_f}{(s - m_R^2)^2 + (m_R\Gamma_R)^2} \quad , \tag{1}$$

where $s = E_{CM}^2$, and m_R and Γ_R are the resonance mass and total width.$^{\|}$ For the $\Upsilon(4S)$, whose decays are almost exclusively to $B\bar{B}$ final states, the leptonic branching ratio is quoted by the Particle Data Group [11] as 1.57×10^{-5} while the total width is 20.5 MeV, leading to a leptonic partial width $\Gamma_{ee} = 0.322$ keV. We shall use this value, noting that it is mildly inconsistent with the Particle Data Group's average of 0.272 keV. The mass is 10.5794 ± 0.0012 GeV; the cross section at the resonance peak is about 2.06 nb. The resonance shape is shown at the left in Fig. 2.

A resonance R may be produced by the radiative return process $e^+e^- \to \gamma R$, where the electron or positron of beam energy $E = E_{CM}/2$ radiates a fraction $1 - x$ of its energy and is left with energy xE. Neglecting the small electron mass, the squared effective mass of the e^+e^- system is then xs. An electron beam of energy E radiates a photon and ends up with an energy xE with a probability per unit x [37] denoted by

$$f_e(x, \sqrt{s}, p_{T,\text{cut}}) = \frac{\alpha}{\pi}\frac{1 + x^2}{1 - x}\ln\frac{E}{p_{T,\text{cut}}} \quad , \tag{2}$$

where the minimum photon transverse momentum $p_{T,\text{cut}}$ provides a collinear cutoff.** In the absence of an explicit choice of cutoff, it is provided by the electron mass m_e, which we shall use in much of what follows. The cross section for production of the resonance R by radiative return, where R decays to the final state f, is then

$$\sigma(e^+e^- \to \gamma R \to \gamma f) = \frac{2\alpha}{\pi}\ln\frac{E}{m_e}\int_0^1 dx\frac{1 + x^2}{1 - x}\sigma(e^+e^- \to R \to f;\ xs) \quad , \tag{3}$$

$^{\|}$An extensive discussion of possible modifications of this expression, including multiplication of Γ by the factor s/m_R^2 to ensure $1/s$ behavior of the cross section at high s, is given in Ref. [36].

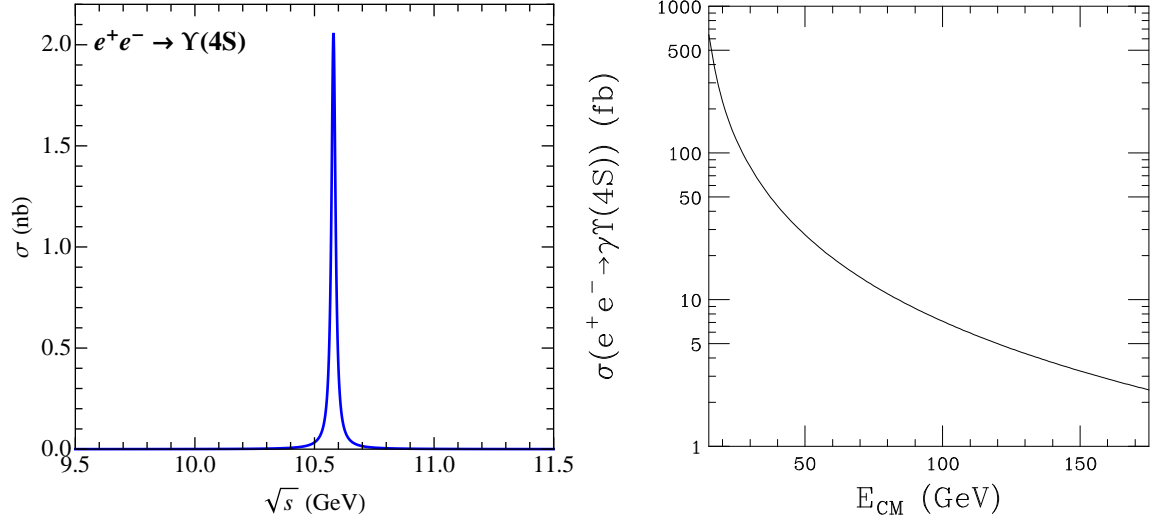**The numerator of the logarithm is sometimes taken to be $2E = \sqrt{s}$.

Figure 2: Cross section for $e^+e^- \to \Upsilon(4S)$ (left) and including the emission of a photon at an e^+e^- collider with CM energy E_{CM} (right).

where the factor of two comes from the fact that either lepton can radiate the photon. In the narrow-resonance approximation, the integral in this expression can be done in closed form, with the result

$$\sigma(e^+e^- \to \gamma R \to \gamma f) \simeq 24\alpha\pi \ln\frac{E}{m_e}\frac{1+x_0^2}{1-x_0}\frac{\Gamma_{ee}\mathcal{B}_f}{m_R\,s} \quad , \tag{4}$$

where $x_0 = m_R^2/s$ and $\mathcal{B}_f = \Gamma_f/\Gamma_R$ denotes the branching fraction into the final state f. The cross section for $e^+e^- \to \Upsilon(4S)$ including the emission of a photon is shown as a function of e^+e^- CM energy in Fig. 2 (right).

The proposed high-energy electron-positron colliders at CERN and in China anticipate integrated luminosities of 50 ab^{-1} and 0.5 ab^{-1}, respectively, at CM energy 90 GeV, and 10 ab^{-1} and 5 ab^{-1}, respectively, at 250 GeV [8,9]. The observation of a new resonance with at least 10 events would then require cross sections of at least 0.2 and 20 ab at CERN or China, respectively, at 90 GeV, or at least 1 and 2 ab, respectively, at 250 GeV.

Fig. 3 illustrates contours of equal cross section for an e^+e^- collider with CM energy 90 (top) and 250 (bottom) GeV to produce a resonance of mass m_R via radiative return. These results imply a cross section of 9.17 fb for the $\Upsilon(4S)$ produced by radiative return at $E_{CM} = 90$ GeV, given an assumed leptonic partial width of $\Gamma_{ee} = 0.322$ keV [11]. For a given E_{CM}, the lowest sensitivity appears to occur for a resonance mass roughly equal to $E_{CM}/2$, i.e., the beam energy.

The results of Fig. 3 can be expressed in more universal form. In the narrow-resonance approximation the predicted radiative return cross section, Eq. (4), is directly proportional to $\Gamma_{ee}\mathcal{B}_f$, so the ratio $\sigma(e^+e^- \to \gamma R \to \gamma f)/\Gamma_{ee}\mathcal{B}_f$ is a function only of s and m_R. In Fig. 4 we plot this ratio as a function of resonance mass for two values of E_{CM}.

The leptonic widths of known and fictitious quarkonium states can serve as benchmarks for the interpretation of Figs. 3 and 4. They are summarized for 1S states in Table III [11,38]. (The bound state of an actual top quark t of mass ~ 173 GeV/c^2 and a $\bar{t}$ is highly unstable due to the weak decay of the t or $\bar{t}$.)
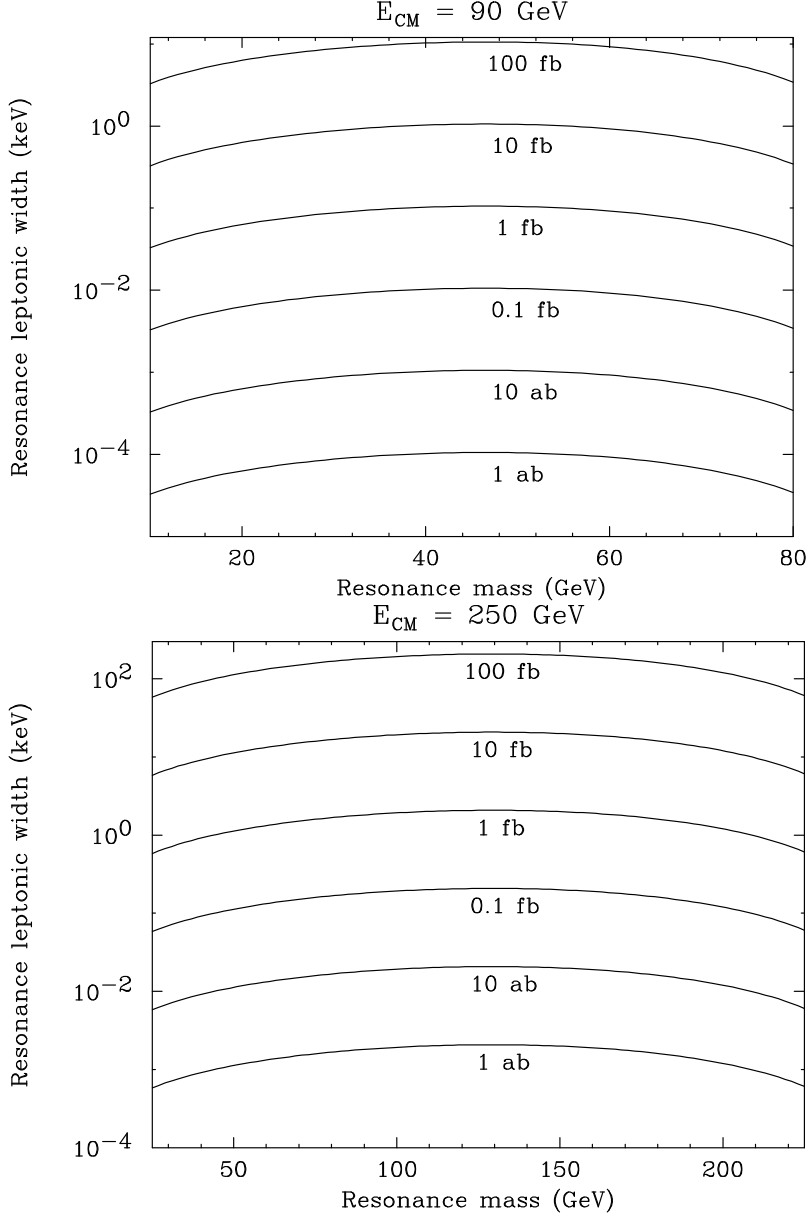
6

Figure 3: Contours of equal cross section for radiative return production of a resonance with leptonic width Γ_{ee} (assuming 100% branching fraction to a final state f). Top: $E_{CM} = 90$ GeV; bottom: $E_{CM} = 250$ GeV.

Table III: Leptonic widths of known and fictitious 1S quarkonium states.

1S state	Quark charge	Quark mass (GeV)	Γ_{ee} (keV)	Ref.
J/ψ	2/3	1.4	$5.55 \pm 0.14 \pm 0.02$	[11]
Υ	−1/3	4.8	1.340 ± 0.018	[11]
Toponium	2/3	40	6.5	[38]
(fictitious)	2/3	45	6.7	[38]

The leptonic width of an S-wave quarkonium $Q\bar{Q}$ bound state of mass M is given by [39]

$$\Gamma_{ee}(Q\bar{Q}) = \frac{16\pi\alpha^2 e_Q^2}{M^2}|\Psi(0)|^2 , \tag{5}$$

where e_Q is the quark charge, $|\Psi(0)|^2$ is the square of the wave function at the origin, and we have neglected relativistic and QCD corrections. One sees that the leptonic widths in Table III are governed primarily by the square of the corresponding quark charge. Over a wide range of quark mass, the decrease of the $1/M^2$ factor is approximately compensated by a corresponding growth of $|\Psi(0)|^2$.

Note that for weakly coupled resonances typically the width is $\propto M$, which needs to be accounted for when interpreting Figs. 3 and 4. In this case the factor of Γ_{ee}/M in Eq. (4) is mostly independent of mass and the cross section is governed purely by the factor $(1 + x_0^2)/(1 - x_0)$, falling monotonically with decreasing resonance mass.

This discussion is oversimplified because it neglects the off-shell process $e^+e^- \to \gamma Z^* \to \gamma R$, in the absence of assumptions about how R couples to Z. However, it gives an idea of the orders of magnitude necessary to find a previously missed resonance in the mass range below that in which the Z^* contributes appreciably (e.g., below about 60 GeV, the CM energy accessible to TRISTAN).

IV   Continuum production

An important quantity is the effective luminosity of a high-energy collider for studying any given process at lower center-of-mass energy. Defining $\sigma(s) \equiv \sigma(e^+e^- \to \gamma f; s)$ and $\hat{\sigma}(\hat{s}) \equiv \sigma(e^+e^- \to f; \hat{s})$ for a given final state f, the relation between the two is

$$\frac{d\sigma(s)}{dx} = \frac{2\alpha}{\pi}\frac{1 + x^2}{1 - x}\ln\frac{E}{m_e}\hat{\sigma}(\hat{s}) , \tag{6}$$

where $x = \hat{s}/s$. The subsystem CM energy may be denoted $\hat{E}_{CM} = \sqrt{\hat{s}}$. The cross section per unit $\hat{E}_{CM}$ times an interval Δ of $\hat{E}_{CM}$ is then

$$\begin{aligned}
\frac{d\sigma(s)}{d\hat{E}_{CM}}\Delta &= \frac{4\alpha\hat{E}_{CM}}{\pi s}\frac{1 + x^2}{1 - x}\Delta\ln\frac{E}{m_e}\hat{\sigma}(\hat{s}) \\
&\equiv L_f\hat{\sigma}(\hat{s}) ,
\end{aligned} \tag{7}$$

where L_f is the *fractional luminosity* per $\hat{E}_{CM}$ bin of size Δ. Examples of this function for a bin width of $\Delta = 1$ GeV are shown in the top curves of Fig. 5.

For low $\hat{E}_{CM}$ one may take $(1 + x^2)/(1 - x) \simeq 1$ in Eq. (7). Integrating from $\hat{E}_{CM}^{\min} = 10$ GeV to $\hat{E}_{CM}^{\max} = 30$ GeV, one then finds

$$L_f = \frac{2\alpha}{\pi s}[(\hat{E}_{CM}^{\max})^2 - (\hat{E}_{CM}^{\min})^2]\ln\frac{E}{m_e} \tag{8}$$

For $E_{CM} = (90, 250)$ GeV we find $L_f = (5.22, 0.74) \times 10^{-3}$. For a total of 1 ab^{-1} at $E_{CM} = (90, 250)$ GeV this then provides a total integrated luminosity of $(5220, 740)$ pb^{-1} in the range $10 \leq \hat{E}_{CM} \leq 30$ GeV. This exceeds integrated luminosities at PEP or PETRA (see Table II).

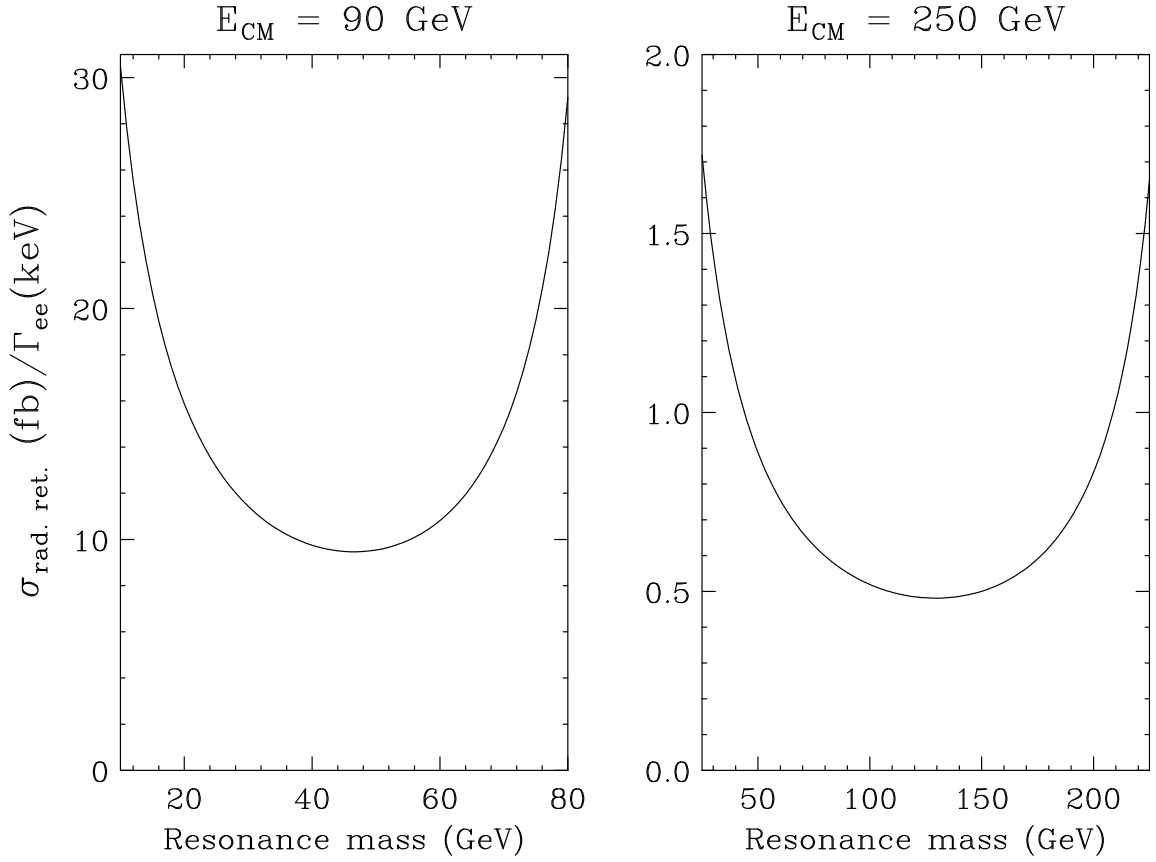Figure 4: $\sigma(e^+e^- \to \gamma R \to \gamma f)/\Gamma_{ee}\mathcal{B}_f$ as a function of resonance mass for $E_{CM} = 90$ (left) and 250 (right) GeV.
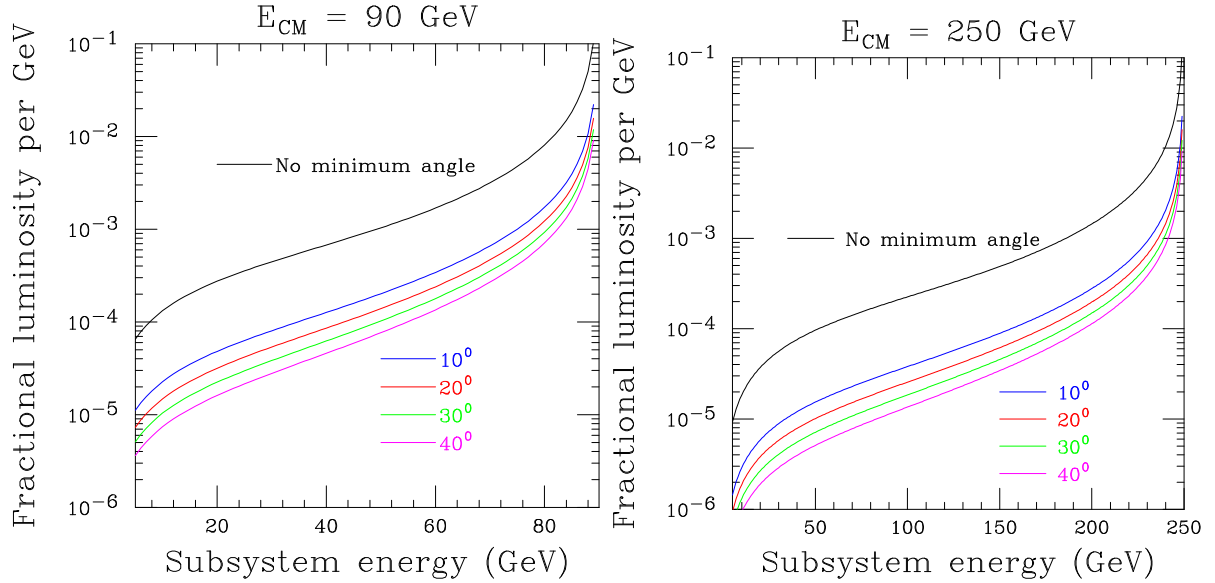

Figure 5: Fractional luminosity L_f as a function of subsystem energy $\hat{E}_{CM}$ for $E_{CM} = 90$ (left) and 250 (right) GeV. Top curves: No minimum angle; infrared cutoff provided by $\ln(E/m_e)$ [Eq. (7)]. Lower curves, top to bottom: $\theta_0 = 10, 20, 30, 40°$.
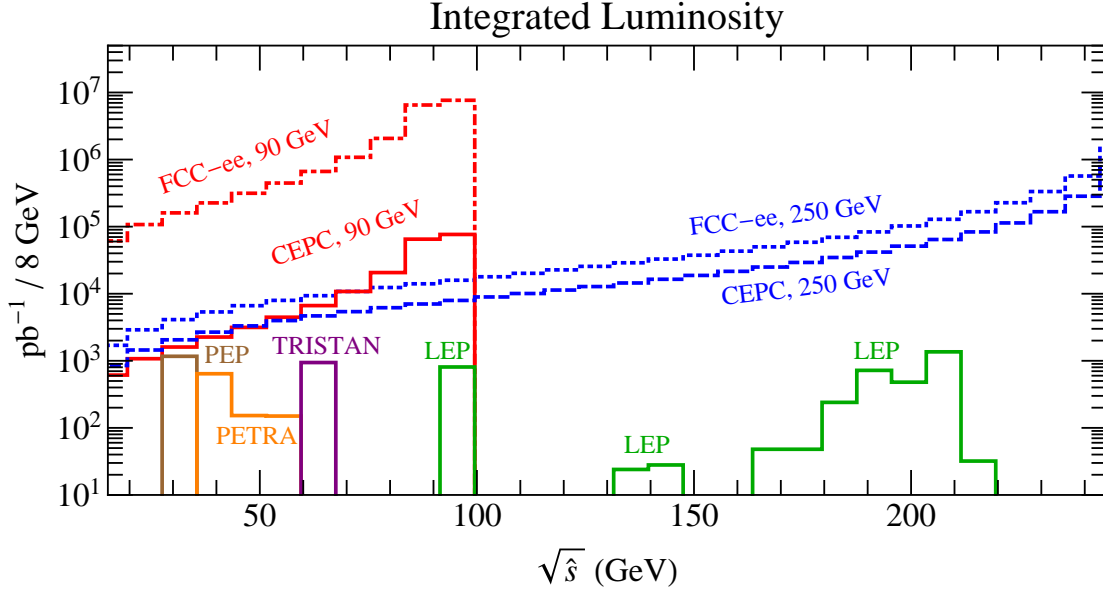
9

Figure 6: Integrated luminosity from past low energy e^+e^- colliders at their nominal center-of-mass energies compared to the effective luminosity through radiative return from future e^+e^- colliders at $\sqrt{s} = 90$ or 250 GeV (no minimum angle; see Fig. 5 for effects of minimum angles). The FCC-ee curves assume an integrated luminosity of 50 ab^{-1} at 90 GeV and 10 ab^{-1} at 250 GeV. The CEPC curves assume an integrated luminosity of 0.5 ab^{-1} at 90 GeV and 5 ab^{-1} at 250 GeV. Integrated luminosities of PEP-II and Belle (Table II) exceed those achievable by radiative return at FCC-ee or CEPC running at 90 or 250 GeV.

Given the concept of fractional luminosity we can compute the effective luminosity gathered at each center-of-mass energy via radiative return. This is shown in Fig. 6 for $\sqrt{s} = 90$ and 250 GeV compared to the luminosity collected directly at various other colliders. In this figure it is illustrated clearly that a high-luminosity high-energy e^+e^- collider both competes with and fills in gaps left by previous colliders.

Cleaner signals for radiative return may be obtained at the expense of recorded events by demanding that the radiated photon make a minimum angle θ_0 with respect to the beam axis. Let θ be the polar angle of the radiated photon, and $z \equiv \cos\theta$, $z_0 \equiv \cos\theta_0$. Using Eq. (8) of [40], we find the angular distribution of the radiated photon for $m_e = 0$ is given by

$$\frac{d^2\sigma(s)}{d\hat{E}_{CM}dz} = \frac{4\alpha\hat{E}_{CM}}{\pi s}\frac{\hat{\sigma}(\hat{s})}{1-z^2}\left[\frac{1-x}{4}(1+z^2) + \frac{x}{1-x}\right] . \tag{9}$$

This may be integrated between the desired limits of θ, with the result

$$\int_{-z_0}^{z_0} dz \frac{d^2\sigma(s)}{d\hat{E}_{CM}dz} = \frac{4\alpha\hat{E}_{CM}}{\pi s}\hat{\sigma}(\hat{s})\left[\frac{1-x}{2}\left(\ln\frac{1+z_0}{1-z_0} - z_0\right) + \frac{x}{1-x}\ln\frac{1+z_0}{1-z_0}\right] . \tag{10}$$

The ratio between the left-hand side and $\hat{\sigma}(\hat{s})$ is again a fractional luminosity and is shown by the lower curves in Fig. 5, again for a bin width of 1 GeV. In the limit of small $\theta_0 \simeq p_T/E_\gamma$, the leading-logarithmic term of Eq. (10) reduces to the form in Eq. (7).

Note that our computation of fractional luminosity utilizes factorization in the collinear limit. In the Appendix, we perform the exact calculation for the process $e^+e^- \to \mu^+\mu^-$ and find good agreement with our results in Fig. 5.

V   Sensitivities of colliders for benchmark processes

We estimate the reach of radiative return studies using electron-positron colliders for two benchmark processes: "dark photon" searches and $b\bar{b}$ production. We compare these sensitivities with those of hadron colliders. Although the latter have an advantage in total rate, it can only be realized with considerable background suppression, such as provided for $b\bar{b}$ production by the VErtex LOcator (VELO) in the LHCb experiment.

A   Dark photon search

In this section we compute the reach for dark photons using radiative return as a concrete example of a search for weakly-coupled resonances. This has been previously computed for GeV-scale dark photons using low energies colliders like PEP-II in [41]. In this work we focus on the 10's to 100's of GeV scale, as discussed in [42]. Other relevant work includes [43–51].

For simplicity, we assume that a "dark photon," denoted by Z', is kinetically mixed with a hypercharge gauge boson with amplitude ϵ

$$\mathcal{L} = -\frac{1}{4}\hat{B}_{\mu\nu}^2 - \frac{1}{4}\hat{Z}_{\mu\nu}'^2 + \epsilon\frac{1}{2c_w}\hat{Z}_{\mu\nu}'\hat{B}^{\mu\nu} + \frac{1}{2}M_{Z'}^2\hat{Z}_\mu'^2 \ , \tag{11}$$

where c_w is the cosine of the Weinberg angle and the hats denote states that are not mass eigenstates. After diagonalization one finds a single massless state, identified to be the photon. The would-be standard model Z and dark photon Z' also mix due to electroweak symmetry breaking. The mixing formulas can be worked out analytically but are not shown here (see [42] for the full expressions).

The dark photon inherits couplings to fermions both from mixing with hypercharge and mixing with the Z. In the limit $\epsilon \ll 1$ and $M_{Z'} \ll M_Z$ the dark photon couplings to fermions become photon-like and the partial width simplifies to

$$\Gamma(Z' \to f\bar{f}) = \frac{\alpha M_{Z'}}{3}Q_f^2 N_c \beta_f \left(\frac{3 - \beta_f^2}{2}\right)\epsilon^2 \ , \tag{12}$$

where there are N_c colors of f with charge Q_f and mass m_f, and

$$\beta_f^2 \equiv 1 - \frac{4m_f^2}{M_{Z'}^2} \ . \tag{13}$$

Ignoring all quark masses except m_b and assuming the top-antitop channel is closed, the branching ratio of Z' into $\mu^+\mu^-$ (a convenient and low-background final state) is

$$\mathcal{B}(Z' \to \mu^+\mu^-) = 3\left(19 + \frac{\beta_b(3 - \beta_b^2)}{2}\right)^{-1} \ . \tag{14}$$

When $M_{Z'} \approx M_Z$ the dark photon couplings become Z-like and when $M_{Z'} \gg M_Z$ they become B-like. This can be seen in Fig. 7 where we show the branching ratios, assuming the dark photon decays entirely into standard model particles. These are computed using $\epsilon = 5 \times 10^{-3}$ although for $\epsilon \ll 1$ the branching ratios are independent of ϵ. For simplicity, we only use the perturbative calculation. For low Z' masses, i.e., below a few GeV, it is necessary to consider threshold effects, QCD corrections, and hadronic resonances.
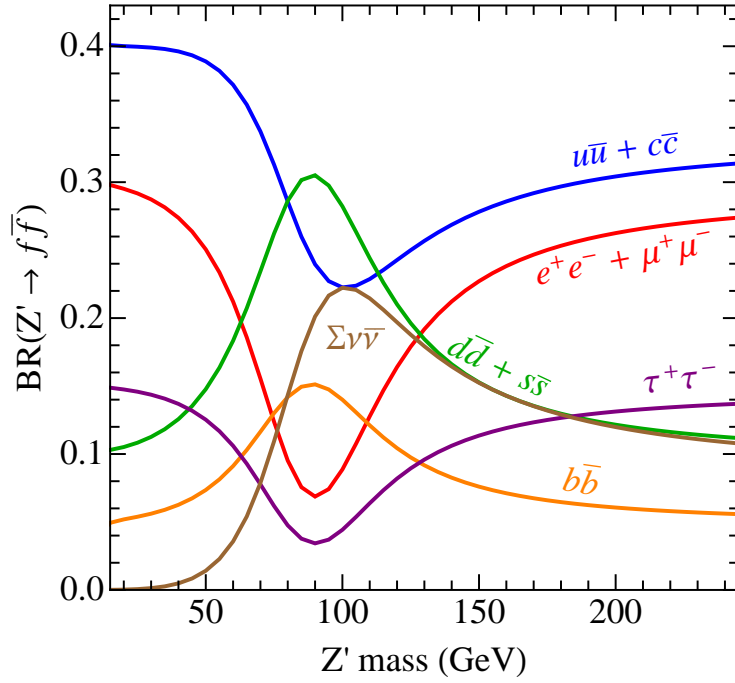
Figure 7: Dark photon branching ratios. These are computed using $\epsilon = 5 \times 10^{-3}$ although for $\epsilon \ll 1$ the branching ratios are independent of ϵ.

A.1 Leptonic production

One recent use of radiative return has been the search by the KLOE Collaboration at the DAΦNE e^+e^- collider for a "dark photon" U decaying to $\mu^+\mu^-$ [18] or e^+e^- [19], produced by the reaction $e^+e^- \to \gamma_{\mathrm{ISR}}U$ at an initial CM energy of about 1 GeV. We make projections for a similar analysis that can be performed for initial CM energies of 90 and 250 GeV.

To compute the reach we consider the background to be $e^+e^- \to \gamma\mu^+\mu^-$ where the muons come from an intermediate γ^* or Z. The search then proceeds by counting the number of events in the dimuon invariant mass spectrum. Since the dark photon width is very narrow the best significance is achieved by binning as narrowly as possible around the targeted Z' mass. The smallest invariant mass bin is determined entirely by the detector's resolution. Typically detector resolution for muon-based searches gets worse at higher momentum (and equivalently higher invariant dimuon mass). We take the mass resolution to be given $\Delta m = m^2/(10^5 \text{ GeV})$ by estimating based on the specification $\Delta(1/p_T) = 2 \times 10^{-5} \text{ GeV}^{-1}$ outlined in future detector designs [52]. [†] For reference, this equates to $\Delta m = 100$ MeV for $m = 100$ GeV. The limit on ϵ scales as $(\Delta m)^{-1/4}$ so a 4 times increase in resolution only results in a 40% increase in reach on ϵ.

The results are shown in Fig. 8. The current and projected limits from electroweak precision data (EWPT) were computed in [42]. Due to some mild tension in the electroweak fit in present data [53] the inclusion of a dark photon with $M_{Z'} > M_Z$ actually improves the fit, which is the reason that projected precision electroweak limits are weaker. Alternative projections that assume the electroweak precision data converges are presented in [42]. At

---

[†]See Appendix A in [41] for an estimation of BaBar's mass resolution. They find the mass resolution to grow quadratically with mass.
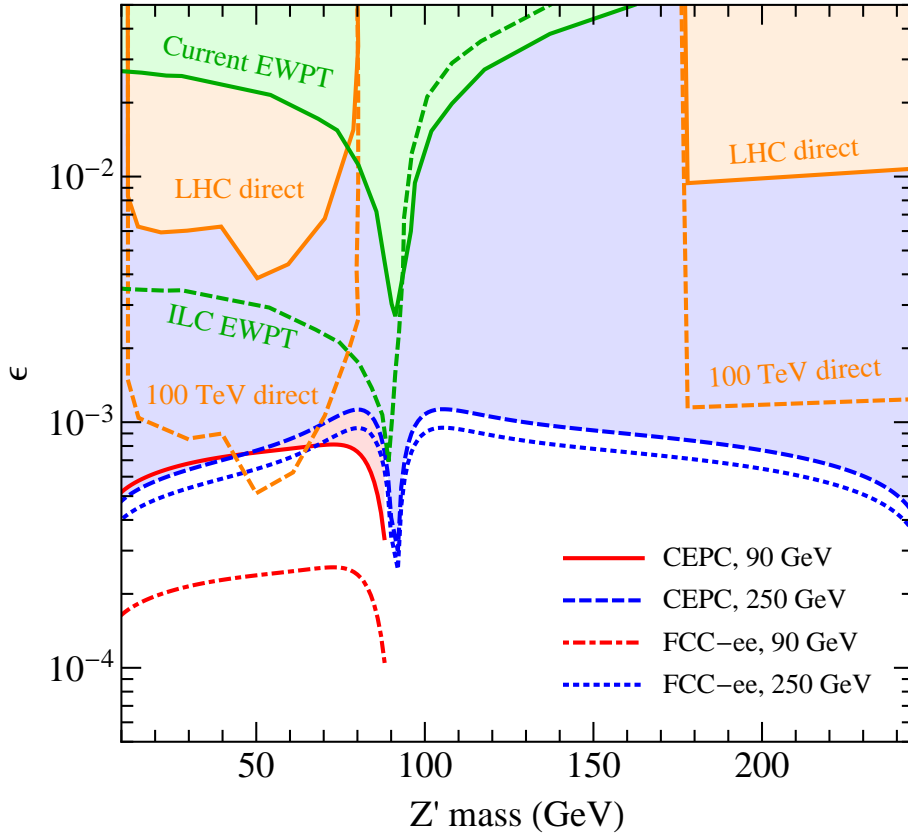
Figure 8: Dark photon limits at 95% C.L. on the hypercharge mixing ϵ as a function of dark photon mass. The $\sqrt{s} = 90$ GeV and 250 GeV lines show our projections with future e^+e^- colliders with integrated luminosities specified in Table I. Electroweak precision constraints (EWPT) and direct searches are taken from [42]. The 100 TeV projection assumes an integrated luminosity of 3000 fb^{-1}.

masses below M_Z, the current direct searches are originally taken from [54] which uses the Drell-Yan process $pp \to Z' \to \ell^+\ell^-$ normalized to 7 TeV LHC data [55] to compute limits using the full 7 and 8 TeV LHC data set.[‡] For direct searches for masses above M_Z, the limits are originally taken from [56], which recast an ATLAS dilepton search [57].[§]. The 100 TeV direct searches are taken from [42] which rescaled the previously mentioned direct limits to 100 TeV with 3000 fb^{-1}.

A.2 Hadronic production

Direct photon production by hadronic collisions in the standard model proceeds through the subprocess $q\bar{q} \to \gamma^*$. Assuming a "dark photon" is produced by this same process, where the γ is now virtual and mixes kinetically with the dark photon Z', one can utilize Drell-Yan production of a lepton pair e^+e^- or $\mu^+\mu^-$ to evaluate the sensitivity of dark photon

---

[‡]For current direct limits on dark photons both above and below M_Z we take limits from [42] rather than from the original studies [54, 56].

[§]As far as we can tell, this limit does not stop at $M_{Z'} \sim 175$ GeV for any fundamental reason, but rather because that is the lowest mass shown in the ATLAS results [57].
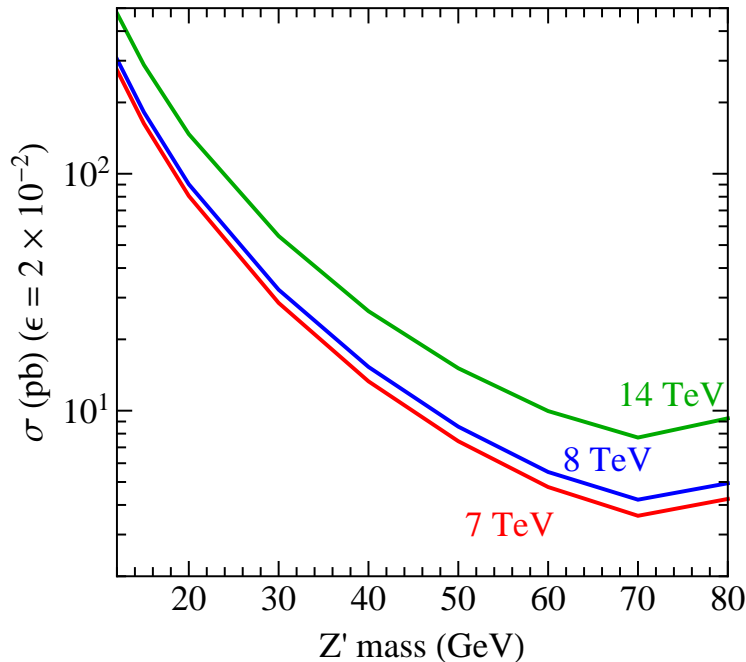
Figure 9: Cross sections for Z' production [54] based on kinetic mixing at a pp collider with CM energy 7 TeV (red), 8 TeV (blue), and 14 TeV (green). Plotted values are to be multiplied by $[\epsilon/(2 \times 10^{-2})]^2 = (50\epsilon)^2$.

searches in hadronic collisions. A sample calculation has been performed in Ref. [54] for various LHC energies; the cross sections are shown in Fig. 9. (The reach of a future 100 TeV pp collider has been investigated in Ref. [42].)

The peaking of parton distributions at low Feynman x favors low Z' masses. For example, at 14 TeV a 15 GeV Z' has a cross section of about $300 \times (2500\epsilon^2)$ pb $= 750\epsilon^2$ nb. Assuming an integrated luminosity of 1 ab^{-1}, this gives rise to at least 10 events when $\epsilon^2 > 1.3 \times 10^{-11}$. At such a low Z' mass, however, background considerations probably dominate any realistic estimate of sensitivity.

B   Production of $b\bar{b}$

B.1   Leptonic production

The asymmetric B factories PEP-II and KEK-B have explored $b\bar{b}$ production up to CM energies of about 11 GeV with compelling statistics, and the upgraded KEK-B with the Belle-II detector will extend samples to dozens of events per attobarn. However, from about 11 to 90 GeV the e^+e^- territory is much more sparsely populated with data, as one can see from Table II and Fig. 6. Radiative return studies from a Giga-Z or Tera-Z factory can help to fill this gap. A sample process is $e^+e^- \to (\gamma^*, Z^*) \to b\bar{b}$, compared for direct production with the radiative return process $e^+e^- \to (\gamma^*, Z^*)\,\gamma_{\text{ISR}} \to b\bar{b}\,\gamma_{\text{ISR}}$.

We use lowest-order MadGraph [58] for our estimates of direct and radiative-return cross sections. For simplicity we assume that the whole PEP sample of 1.167 events per fb is accumulated at $\sqrt{s} = 29$ GeV, where MadGraph predicts $\sigma(e^+e^- \to b\bar{b}) = 36.8$ pb, giving a total sample of about 43k events. The corresponding cross sections at 35 and 60 GeV,

Table IV: Comparison of direct and radiative-return e^+e^- production of $b\bar{b}$.

Collider	Direct			Radiative return				
	σ	$\int \mathcal{L}dt$	Events	$\hat{E}$ range	$\sqrt{s} = 90$ GeV		$\sqrt{s} = 250$ GeV	
	(pb)	(pb^{-1})	(10^3)	(GeV)	σ (pb)	Evts.$(10^6)^a$	σ (pb)	Evts.$(10^3)^b$
PEP	36.8	1167	42.9	10–35	0.494	(24.5,0.245)	0.066	(660,330)
PETRA	25.8	817	21.1	35–60	0.410	(20.5,0.205)	0.039	(391,196)
TRISTAN	16.2	942	15.3	60–85	12.94	(647,6.47)	0.256	(2562,1281)

[a] Assuming $\int \mathcal{L}dt = (50, 0.5)$ ab^{-1} at (FCC-ee, CEPC).
[b] Assuming $\int \mathcal{L}dt = (10, 5)$ ab^{-1} at (FCC-ee, CEPC).

relevant for PETRA and TRISTAN, are 25.8 and 16.2 pb, respectively. With integrated luminosities of 817 and 942 events per pb (Table II), one then has respective samples of 21.1k and 15.3k events from the direct process at PETRA and TRISTAN.

For radiative return we consider samples integrated over the $\hat{E}_{CM}$ ranges [10,35], [35,60], and [60,85] GeV, applying Eq. (7) and recalling that the beam energy E is $\sqrt{s}/2$.[¶] The results are compared with the direct process in Table IV.

Even if all the data from PEP, PETRA, and TRISTAN are pooled, they are less than the sample that would be gained in the $\hat{E}_{CM}$ range from 10 to 60 GeV by studying radiative return from an e^+e^- collider at $\sqrt{s} = 90$ or 250 GeV.

B.2 Hadronic production

It is not straightforward to compare leptonic and hadronic $b\bar{b}$ production because the background circumstances are different. However, the LHCb Collaboration has demonstrated great sensitivity to specific final states in which backgrounds can be largely overcome. As one example, a recent study of b hadron lifetimes [59] based on a data sample of 1 fb^{-1} at $\sqrt{s} = 7$ TeV accumulates a sample of $229,439 \pm 503$ $B^+ \to J/\psi K^+$ events, with J/ψ decaying to $\mu^+\mu^-$. Given the branching fractions $\mathcal{B}(B^+ \to J/\psi K^+) = (1.027 \pm 0.031) \times 10^{-3}$ and $\mathcal{B}(J/\psi \to \mu^+\mu^-) = (5.93 \pm 0.06)\%$ [11], this corresponds to about $(3.77 \times 10^9)/\epsilon_f$ B^+ produced, where $\epsilon_f < 1$ is the acceptance for the final state f in question. In fact, the production cross sections for B mesons at the LHC have been measured [60]:

$$\sigma(pp \to B^+ + X) = (38.9 \pm 0.3 \pm 2.5 \pm 1.3)\mu\text{b} , \tag{15}$$
$$\sigma(pp \to B^0 + X) = (38.1 \pm 0.6 \pm 3.7 \pm 4.7)\mu\text{b} , \tag{16}$$
$$\sigma(pp \to B_s + X) = (10.5 \pm 0.2 \pm 0.8 \pm 1.0)\mu\text{b} , \tag{17}$$

where the errors are statistical, systematic, and normalization (based on prior branching fraction measurements). This would correspond to about 3.9×10^{10} B^+ in a sample of 1 fb^{-1}, yielding an estimate of $\epsilon_f \simeq 10\%$.

[¶]In MadGraph the logarithm is taken to be $\ln(\sqrt{s}/P_{T,\text{cut}})$; we apply corresponding corrections of 0.9426 and 0.9471 to the MadGraph results at $\sqrt{s} = 90$ and 250 GeV.

VI   Some accessible questions in heavy flavor spectroscopy

Much progress in heavy flavor spectroscopy has been made using the B factories PEP-II and KEK-B. However, these machines were limited, as will be the KEK-B upgrade, to CM energies not much above 11 GeV. There are a number of questions in the spectroscopy of hadrons containing heavy (charm and bottom) quarks that could benefit from higher CM energies. Can an e^+e^- collider with CM energy 250 GeV and luminosity 10^{34} cm^{-2}s^{-1} provide integrated luminosity to study such states significantly above what has already been provided by PEP, PETRA, TRISTAN, and LEP? A sharper answer can be provided by considering specific processes.

A   Bottomonium analogues of charmonium X, Y, and Z states

There are a number of charmonium states that appear to contain extra light quarks or to be admixtures of $c\bar{c}$ and charmed meson pairs. Some analogues of these have been seen in the bottomonium sector, but so far the X_b, the analogue of the $X(3872)$, has eluded clearcut detection. There is an intriguing possibility that X_b might have already been observed, but identified as $\chi_{b1}(3P)$ which is close in mass and has the same quantum numbers [61]. Electron-positron collisions with CM energy greater than 11 GeV may be helpful in resolving this issue and allowing for unambiguous identification of X_b and related states.

B   Pair production of narrow B_{sJ} states

The reaction $e^+e^- \to B_{sJ} + X$ may be used to look for the b-quark analogue of the very narrow D_{sJ} states seen by BaBar, CLEO and Belle [62–64]. The relevant thresholds are discussed in Subsection D below.

C   Doubly heavy flavor production

With sufficient CM energy one may study such processes as

$$
\begin{aligned}
e^+e^- &\to b\bar{b}c\bar{c} + X \ , \\
e^+e^- &\to b\bar{b}b\bar{b} + X \ ,
\end{aligned}
\tag{18}
$$

as a precondition for producing doubly heavy mesons such as B_c, B_c^*, and doubly heavy baryons such as $\Xi_{bc} = bcq$, and $\Xi_{bb} = bbq$, where q is a light quark. Until now the latter have never been clearly observed, even though it is clear they must exist. As shown in Ref. [65], one must be able to see the (known) B_c state if one expects to be able to detect Ξ_{bc}, so we shall estimate B_c production by radiative return. We shall consider the case $E_{CM} = 90$ GeV, assuming that a circular e^+e^- collider will spend some time as a Giga- (or Tera-) Z factory.

The mass of B_c is by now very well known [11]: $M(B_c) = 6275.6 \pm 1.1$ MeV. For optimal B_c production, one probably needs to be above $B_c^{*+}B_c^{*-}$ threshold, which according to the estimate of Ref. [65] lies between 12.69 and 12.72 GeV. The cross section $\sigma(e^+e^- \to$

$B_c^{*+} B_c^{*-}$) probably rises sharply near threshold, in the same manner as $\sigma(e^+ e^- \to D^{*+} D^{*-})$, and may be estimated as follows.

The cross section for $e^+ e^-$ production of a $b\bar{b}$ pair, far enough above the $\Upsilon(4S)$, is expected to be

$$\sigma(e^+ e^- \to b\bar{b}; \hat{s}) = \frac{4\pi\alpha^2}{3\hat{s}} \cdot \frac{1}{3} = \frac{4\pi\alpha^2}{3s} \cdot \frac{1}{x} \cdot \frac{1}{3} \ , \tag{19}$$

and is about 180 pb at $\sqrt{\hat{s}} = 12.72$ GeV. By comparing cross sections for B^+ and B_c production at LHCb, Ref. [65] found the probability of a b quark fragmenting to $B_c^- = b\bar{c}$ to be about 10^{-2}. Thus near $B_c^{*+} B_c^{*-}$ threshold, one might expect

$$\sigma(e^+ e^- \to B_c^+ B_c^- + X) \simeq 1.8 \text{ pb} \ , \tag{20}$$

where X denotes the possibility of one or two additional photons from B_c^* decays.

The cross section, Eq. (19), may now be multiplied by $2f_e(x, \sqrt{s}, p_{T,\text{cut}})$ (see Eq. (2)) and integrated over an appropriate range of x. The B_c^* form factor and the $1/\hat{s}$ factor in the cross section will introduce some suppression, which we shall imitate by introducing a maximum $\hat{s}_{\max} = (20 \text{ GeV})^2$. For $E_{CM} = 90$ GeV, we thus perform the integral

$$\sigma(e^+ e^- \to \gamma B_c^+ B_c^- + X) = \frac{2\alpha}{\pi} \ln \frac{E}{m_e} \int \frac{dx}{x} (35.7 \text{ fb}) = 1.7 \text{ fb} \ . \tag{21}$$

Here we have neglected the small deviation of $(1 + x^2)/(1 - x)$ from 1, taken the limits of integration between $x_{\min} = (12.72/90)^2$ and $x_{\max} = (20/90)^2$, and used $E = 45$ GeV. One still has to pay the price of the B_c branching fraction to an observable final state, but as we expect $\mathcal{B}(B_c \to J/\psi\mu\nu)$ to exceed a percent [65] this seems possible with a sample exceeding one event per ab.

At a different center-of-mass energy, as long as the same range of $\sqrt{\hat{s}}$ is taken, one can show that the cross section in Eq. (21) scales as $(1/s) \ln(E/m_e)$, so at $\sqrt{s} = 250$ GeV, it becomes 0.24 fb.

D Interesting thresholds

The production of $B\bar{B}$ pairs has occupied most of the running time of the B factories KEK-B and PEP-II. However, some data have been taken at higher energies, as indicated in Table II. The CLEO Collaboration has taken a small amount of data above $\Lambda_b \bar{\Lambda}_b$ threshold in search of a "magic energy" for Λ_b pair production; none was found. In Table V we summarize some thresholds for heavy flavor production in $e^+ e^-$ collisions.

Here we have used masses tabulated in Ref. [11]. The state B_{s0} in Table V is the expected analogue, with $J^P = 0^+$, of the $D_{s0}(2317)$, which is narrow because it lies below DK threshold. In order to produce the B_{s0} in $e^+ e^-$ collisions, it must be accompanied by a $\bar{B}_s^*$ or heavier companion. Angular momentum and parity conservation forbid the process $e^+ e^- \to \gamma^* \to B_{s0} \bar{B}_s$. The B_{s0} mass is estimated to be 5717 MeV by assuming that D_{s0} and D_{s0} are chiral partners of D_s and B_s and therefore the $B_{s0} - B_s$ splitting is very close to the $D_{s0} - D_s$ splitting [66, 67]. On the other hand, in order for B_{s0} to be interesting, it needs to be narrow. In analogy with D_{s0} which is narrow because it is below the DK threshold, B_{s0} needs to be below BK threshold, i.e., below 5778 MeV. So in any case the interesting threshold is between 5717 MeV $+ m_{B_s^*}$ and 5778 MeV $+ m_{B_s^*}$, i.e., between 11132 MeV and 11193 MeV.

Table V: Some thresholds for heavy flavor production in e^+e^- collisions.

Final state	Threshold (MeV)
$B\bar{B}$	10559
$B\bar{B}^*$	10605
$B^*\bar{B}^*$	10650
$B_s\bar{B}_s$	10734
$B_s\bar{B}_s^*$	10782
$B_s^*\bar{B}_s^*$	10831
$B_{s0}\bar{B}_s^*$	11132–11193[a]
$\Lambda_b\bar{\Lambda}_b$	11239
$B_c\bar{B}_c$	12551
$B_c\bar{B}_c^*$	12619–12635[b]
$B_c^*\bar{B}_c^*$	12687–12719[b]
$\Xi_{bc}\bar{\Xi}_{bc}$	13842–13890[c]
$\Xi_{bb}\bar{\Xi}_{bb}$	20300–20348[c]

[a]See text. [b]With estimated B_c^*–B_c splitting 68–84 MeV [65]. [c] Estimate in [65].

VII   Conclusions

While e^+e^- collisions have been studied with impressive statistical power at energies accessible to the asymmetric B factories KEK-B and PEP-II, the CM energy range from about 12 to 80 GeV accessible to PEP, PETRA, and TRISTAN is much less thoroughly investigated. The radiative return process $e^+e^- \to \gamma_{\text{ISR}}e^+e^- \to \gamma_{\text{ISR}}f$, where ISR denotes initial-state radiation, can help fill this gap. Some examples are given of processes that could be investigated using radiative return, starting from a collider operating at 90 or 250 GeV. Although the same final states f can often be produced with higher cross sections in hadronic collisions, the relative cleanliness of the e^+e^- environment gives it an advantage whose quantitative value must be investigated using detailed detector simulation.

Processes which could benefit from radiative return studies at high energies include searches for "dark photons" Z', heavy quark (particularly b) production, and spectroscopy of states too heavy to be produced at the asymmetric B factories. In studying subenergies in the 12–80 GeV range, it was found advantageous to use total e^+e^- CM energies near the Z rather than at the highest possible energy.

ing Center at the University of Chicago.

VIII   Appendix: Parton luminosity

Another way to understand the rate for a process below the nominal center-of-mass energy is using parton luminosities [68,69]. In this parameterization the cross section is written as

$$
\begin{aligned}
\sigma(s) &= \int d\tau \frac{dL_{ab}}{d\tau} \hat{\sigma}_{ab}(\hat{s}) , \\
&= \int \frac{d\tau}{\tau} \left(\frac{1}{s} \frac{dL_{ab}}{d\tau} \right) [\hat{s}\hat{\sigma}_{ab}(\hat{s})] ,
\end{aligned}
\tag{22}
$$

where $\tau = \hat{s}/s$ and a,b specify the incoming parton species. The hatted quantities are with respect to the colliding partons, primarily electron and photons for e^+e^- colliders and quarks and gluons for pp or $p\bar{p}$ colliders. The quantity $(1/s)(dL_{ab}/d\tau)$ is called the *parton luminosity* and has units of a cross section. It is computed as

$$
\frac{dL_{ab}}{d\tau} = \frac{1}{1+\delta_{ab}} \int_\tau^1 \frac{dx}{x} \left[f_a(x) f_b\left(\frac{\tau}{x}\right) + f_a\left(\frac{\tau}{x}\right) f_b(x) \right] .
\tag{23}
$$

In the following subsections we show the parton luminosity calculated for lepton colliders and hadron colliders as a means to compare the expected rates at the different types of colliders. An important caveat is to note that there are significant differences to actually computing rates at the different machines which means just comparing the parton luminosity values can give an inaccurate picture. More realistically one needs to consider leptonic versus hadronic branching ratios, detector efficiencies for the final states, and background processes.

A   Leptonic parton luminosity

At an e^+e^- collider when considering the only initial state as e^+e^- and not $e^+\gamma$, $e^-\gamma$, or $\gamma\gamma$, the electron distribution function is almost the same as the splitting function $f_e(x)$ in Eq. (2):

$$
f_e(x,s) = \delta(1-x) + \frac{\alpha}{\pi} \ln \frac{E}{m_e} \left(\frac{1+x^2}{(1-x)_+} + \frac{3}{2}\delta(1-x) \right) + \mathcal{O}(\alpha^2) .
\tag{24}
$$

The plus distribution regularizes the behavior at $x = 1$ [70] and the $(3/2)\delta(1-x)$ is for overall normalization. The inclusion of the δ-function is necessary because the distribution function is inclusive and needs to account for the no-splitting case.

For the parton luminosity we find

$$
\frac{dL}{d\tau} = \delta(1-\tau)\left(1 + \frac{3\alpha}{\pi}\ln\frac{E}{m_e} + \mathcal{O}(\alpha^2)\right) + \frac{2\alpha}{\pi}\ln\frac{E}{m_e}\frac{1+\tau^2}{1-\tau} + \mathcal{O}(\alpha^2).
\tag{25}
$$

Fig. 10 (left) shows the parton luminosity for several different CM energies. For narrow resonances, we can directly use the parton luminosity to compute rates. According to the narrow width approximation for a resonance of spin J, mass m, and total width Γ

$$
\hat{s}\hat{\sigma}(\hat{s}) = 4\pi^2(2J+1)\mathcal{B}_i\mathcal{B}_f m\Gamma\delta(\hat{s}-m^2) ,
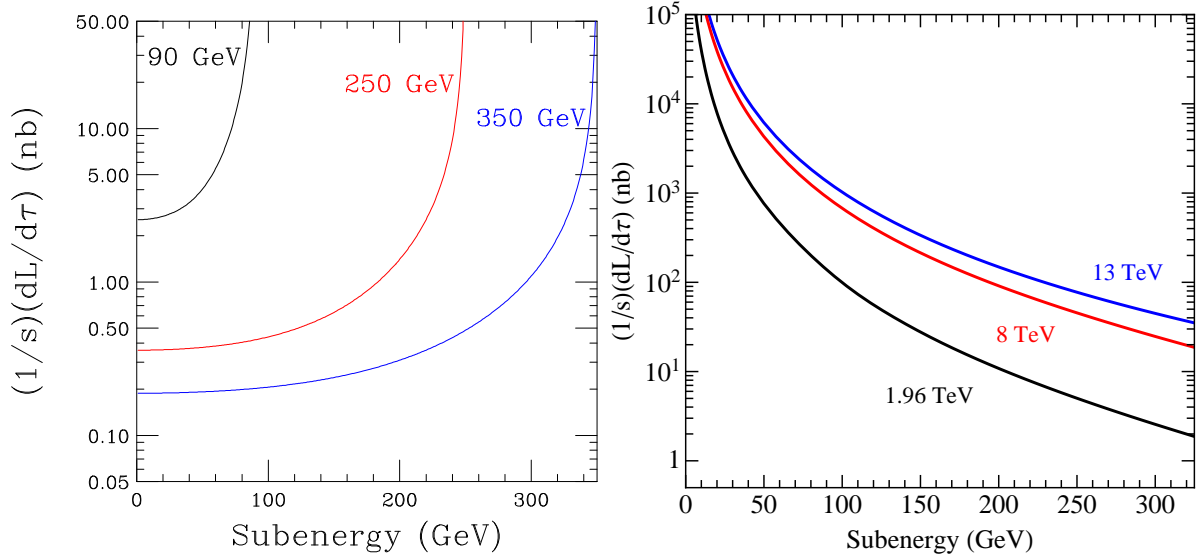\tag{26}
$$

19

Figure 10: Parton luminosities for e^+e^- at $\sqrt{s} = 90$ GeV, 250 GeV, 350 GeV (left) and for $p\bar{p}$ at $\sqrt{s} = 1.96$ TeV and pp at $\sqrt{s} = 8$ TeV, 13 TeV (right).

giving a cross section of

$$\sigma(s) = 4\pi^2(2J+1)\mathcal{B}_f \frac{\Gamma_i}{m}\left(\frac{1}{s}\frac{dL}{d\tau}\right)\Bigg|_{\tau=m^2/s}. \tag{27}$$

We can evaluate the appropriate s curve in Fig. 10 at a subenergy m and find the rate by multiplying by Γ/m, a spin factor, and branching ratios. As an example, with $\Gamma_{ee} = 0.322$ keV and $m = 10.5794$ GeV, we find $\sigma(e^+e^- \to \gamma\Upsilon(4S); s = (90 \text{ GeV})^2) = 9.17$ fb, the value obtained in Section III.

B   Hadronic parton luminosity

For comparison we consider a hadron collider with the initial state

$$q\bar{q} = \{u\bar{u}, d\bar{d}, s\bar{s}, c\bar{c}, \bar{u}u, \bar{d}d, \bar{s}s, \bar{c}c\}. \tag{28}$$

The parton distribution functions for the proton are non-perturbative functions that describe the probability a given parton is taken from the proton.

Fig. 10 (right) shows the parton luminosity for several different CM energies. In contrast to lepton colliders, a higher-energy hadron collider also increases the rates at lower subenergies.

The parton distributions are accessed via the LHAPDF interface [71]. The sets used are `CT10nnlo_as_0118` set [72], `MTSW2008nnlo68cl` [68], and `NNPDF23_nnlo_as_0118` [73]. Only the `CT10` set is shown in Fig. 10 as the differences are negligible in the figure.

IX   Appendix: Fractional luminosity for $e^+e^- \to \mu^+\mu^-$

In Section IV we discussed fractional luminosity using factorization in the collinear limit to compute $\sigma(s) \equiv \sigma(e^+e^- \to \gamma f; s)$ in terms of $\sigma(e^+e^- \to f; s)$ with the results shown in
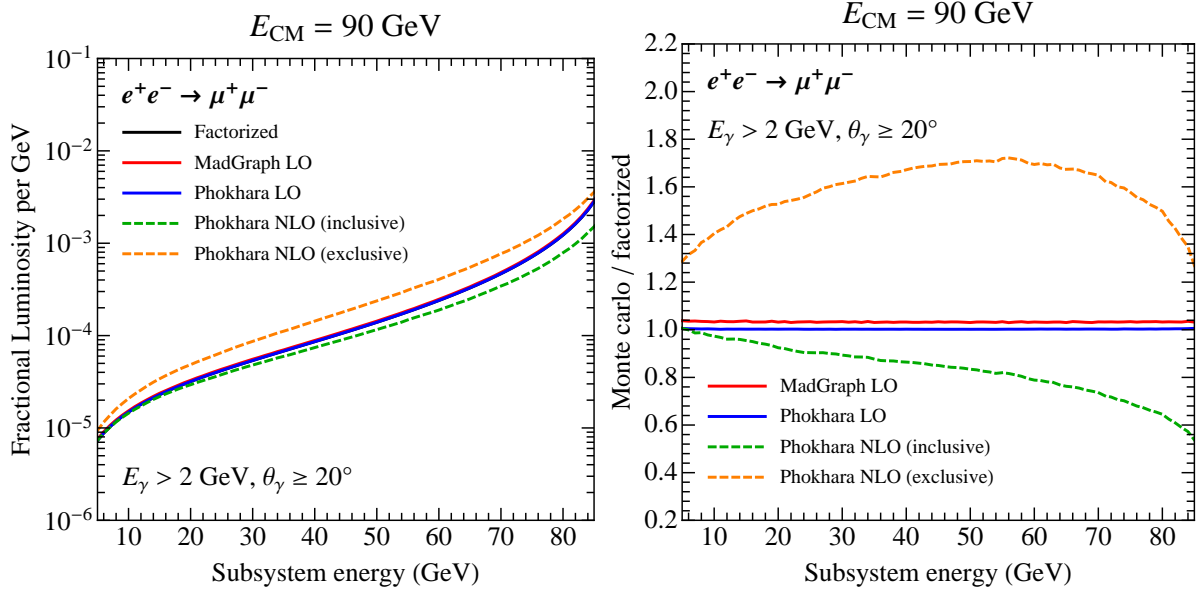
20

Figure 11: Fractional luminosity for process $e^+e^- \rightarrow \mu^+\mu^-$ at $\sqrt{s} = 90$ GeV with an angular cut of 20° (left) and showing the difference between the Monte Carlo and analytic calculation (right). A bin size of $\Delta = 1$ GeV is used.

Fig. 5. The use of factorization is very convenient to obtain general results independent of the final state f.

Here we compute the fractional luminosity exactly with the processes $\sigma(e^+e^- \rightarrow \mu^+\mu^-; s)$ and $\sigma(e^+e^- \rightarrow \gamma\mu^+\mu^-; s)$ to demonstrate that the factorized form used in the main text was justified. We use the Monte Carlo programs MadGraph [58] and Phokhara [74]. Fig. 11 (left) shows the fractional luminosity compared to our computation from Section IV for $\theta_\gamma \geq 20°$ and $E_\gamma > 2$ GeV. The energy cutoff is necessary to cut off the soft divergence. Fig. 11 (right) shows the ratio of the Monte Carlo to the analytic factorized form. The Phokhara result agrees well with the factorized form and the MadGraph results differ in normalization by $\approx 5\%$. Results for other angular cuts are similar.

Fig. 11 also displays next-to-leading (NLO) order results computed with Phokhara. Interpreting these results requires some additional explanation. Recall the definition of fractional luminosity

$$\frac{d\sigma(s)}{d\hat{E}_{CM}}\Delta \equiv L_f\hat{\sigma}(\hat{s}) , \qquad (29)$$

where $\sigma(s)$ is the three-body cross section and $\hat{\sigma}(\hat{s})$ is the two-body cross section.

Explicitly, the left side of Eq. (29) evaluates the differential three-body distribution at a given $\hat{E}_{CM}$ value and is multiplied by the bin width Δ to get a three-body cross section (i.e., one term of a Riemann sum). The right side of Eq. (29) is the two-body cross section evaluated at $\hat{E}_{CM}^2 = \hat{s}$ with a coefficient identified as the fractional luminosity.

At leading order (LO), this definition is unambiguous because the two-body cross section is a δ-function in $\hat{s}$. At NLO, however, the two-body cross section becomes a distribution in $\hat{s}$ due to real photon emission.$^{\|}$ One needs to choose whether to define the two-body

---

$^{\|}$Considering real emission an N-body process becomes an $N+1$-body process, but for simplicity we

cross section as the integral over all $\hat{s}$ values or the integral over a small window Δ near the nominal value.

The former we call the *inclusive* NLO cross section and evaluate as

$$\hat{\sigma}(\hat{E}_{CM}) = \int_0^{\hat{E}_{CM}} \left(\frac{d\hat{\sigma}}{d\hat{E}'_{CM}}\right) d\hat{E}'_{CM} , \tag{30}$$

and the latter we call the *exclusive* NLO cross section

$$\hat{\sigma}(\hat{E}_{CM}) = \int_{\hat{E}_{CM}-\Delta}^{\hat{E}_{CM}} \left(\frac{d\hat{\sigma}}{d\hat{E}'_{CM}}\right) d\hat{E}'_{CM} . \tag{31}$$

Both versions are shown in Fig. 11 in green (lower) and orange (upper) dashed lines, respectively.

The inclusive result has a lower fractional luminosity because the two-body cross section is larger than the LO result. This is because the real photon emission already induces some radiative return. The decrease of the fractional luminosity, relative to LO, at high subenergies is due to the three-body cross section decreasing because of the 2 GeV cut on photon energy.

On the other hand, the exclusive result has a lower two-body cross section because the integration only includes values of $\hat{E}_{CM}$ near the nominal value while the phase space at lower values is still populated. The three-body cross section is the same as the inclusive case so the same decrease at high subenergies is observed. The exclusive result depends on the bin size used. In Fig. 11 we show results using a bin size of $\Delta = 1$ GeV. As the bin size is increased, the exclusive result approaches the inclusive result.

References

[1] A. Denig, Nucl. Phys. Proc. Suppl. **162**, 81 (2006) [hep-ex/0611024].

[2] W. Kluge, Nucl. Phys. Proc. Suppl. **181-182**, 280 (2008) [arXiv:0805.4708 [hep-ex]].

[3] H. Czyz, A. Grzelinska, and J. H. Kuhn, Phys. Rev. D **81**, 094014 (2010) [arXiv:1002.0279 [hep-ph]].

[4] V. P. Druzhinin, S. I. Eidelman, S. I. Serednyakov, and E. P. Solodov, Rev. Mod. Phys. **83**, 1545 (2011) [arXiv:1105.4975 [hep-ex]].

[5] See http://cern.ch/fcc-ee

[6] See http://cepc.ihep.ac.cn; *Physics World*, Aug. 26, 2014.

[7] For a discussion of this possibility see M. Ruan, "Higgs measurement at e^+e^- circular colliders", report at ICHEP 2014, Valencia, Spain, arXiv:1411.5606 [hep-ex].

[8] CEPC-SPPC Prelimary Conceptual Design Report, *to appear*.

[9] M. Bicer *et al.* [TLEP Design Study Working Group Collaboration], J. High Energy Phys. 01 (2014) 164 [arXiv:1308.6176 [hep-ex]].

will label it by its LO phase space, so that even with real emission it is called an N-body process.

[10] J. Fan, M. Reece, and L. T. Wang, arXiv:1411.1054 [hep-ph].

[11] K. A. Olive *et al.* (Particle Data Group), Chin. Phys. C **38**, 090001 (2014).

[12] R. M. Barnett *et al.* (Particle Data Group Collaboration), Phys. Rev. D **54**, 1 (1996).

[13] C. Biscari, eConf C **0309101**, THWA001 (2003) [arXiv: physics/0401031].

[14] A. Aloisio *et al.* (KLOE Collaboration), Phys. Lett. B **606**, 12 (2005) [hep-ex/0407048].

[15] F. Ambrosino *et al.* (KLOE Collaboration), Phys. Lett. B **670**, 285 (2009) [arXiv:0809.3950 [hep-ex]].

[16] D. Babusci *et al.* (KLOE Collaboration), Phys. Lett. B **720**, 336 (2013) [arXiv:1212.4524 [hep-ex]].

[17] F. Ambrosino *et al.* (KLOE Collaboration), Phys. Lett. B **700**, 102 (2011) [arXiv:1006.5313 [hep-ex]].

[18] F. Curciarello, Acta Physica Polonica B vol. 46 (2015) [arXiv:1501.04424 [hep-ex]].

[19] A. Palladino, arXiv:1501.05173 [hep-ex].

[20] S. Dobbs *et al.* (CLEO Collaboration), Phys. Rev. Lett. **94**, 032004 (2005) [hep-ex/0410038].

[21] J. P. Lees *et al.* (BaBar Collaboration), Phys. Rev. D **85**, 112009 (2012) [arXiv:1201.5677 [hep-ex]].

[22] J. P. Lees *et al.* (BaBar Collaboration), Phys. Rev. D **86**, 012008 (2012) [arXiv:1103.3001 [hep-ex]].

[23] J. P. Lees *et al.* (BaBar Collaboration), Phys. Rev. D **86**, 032013 (2012) [arXiv:1205.2228 [hep-ex]].

[24] J. P. Lees *et al.* (BaBar Collaboration), Phys. Rev. D **86**, 051102 (2012) [arXiv:1204.2158 [hep-ex]].

[25] J. P. Lees *et al.* (BaBar Collaboration), Phys. Rev. D **87**, 092005 (2013) [arXiv:1302.0055 [hep-ex]].

[26] J. P. Lees *et al.* (BaBar Collaboration), Phys. Rev. D **88**, 032013 (2013) [arXiv:1306.3600 [hep-ex]].

[27] J. P. Lees *et al.* (BaBar Collaboration), Phys. Rev. D **89**, 111103 (2014) [arXiv:1211.6271 [hep-ex]].

[28] J. P. Lees *et al.* (BaBar Collaboration), Phys. Rev. D **89**, 092002 (2014) [arXiv:1403.7593 [hep-ex]].

[29] C. P. Shen *et al.* (Belle Collaboration), Phys. Rev. D **89**, 072015 (2014) [arXiv:1402.6578 [hep-ex]].

[30] X. L. Wang, *et al.* (Belle Collaboration), arXiv:1410.7641 [hep-ex].

[31] R. Barate *et al.* (ALEPH Collaboration), Phys. Lett. B **399**, 329 (1997).

[32] P. Abreu *et al.* (DELPHI Collaboration), Z. Phys. C **75**, 581 (1997).

[33] M. Acciarri *et al.* (L3 Collaboration), Phys. Lett. B **374**, 331 (1996).

[34] P. D. Acton *et al.* (OPAL Collaboration), Phys. Lett. B **273**, 338 (1991).

[35] G. Abbiendi *et al.* (OPAL Collaboration), Phys. Lett. B **604**, 31 (2004) [hep-ex/0408130].

[36] LEP (ALEPH, DELPHI, L3, and OPAL) Line Shape Sub-Group of the LEP Electroweak Working Group Collaboration, hep-ex/0101027. See also S. Mrenna, http://home.fnal.gov/~mrenna/lutp0613man2/node74.html, unpublished.

[37] M. S. Chen and P. M. Zerwas, Phys. Rev. D **12**, 187 (1975).

[38] P. Moxhay and J. L. Rosner, Phys. Rev. D **31**, 1762 (1985).

[39] R. Van Royen and V. F. Weisskopf, Nuovo Cim. A **50**, 617 (1967) [Erratum-ibid. A **51**, 583 (1967)].

[40] M. S. Chen and P. M. Zerwas, Phys. Rev. D **11**, 58 (1975).

[41] M. Reece and L. T. Wang, J. High Energy Phys. 07 (2009) 051 [arXiv:0904.1743 [hep-ph]].

[42] D. Curtin, R. Essig, S. Gori, and J. Shelton, arXiv:1412.0018 [hep-ph].

[43] M. Pospelov, A. Ritz, and M. B. Voloshin, Phys. Lett. B **662**, 53 (2008) [arXiv:0711.4866 [hep-ph]].

[44] N. Arkani-Hamed and N. Weiner, J. High Energy Phys. 12 (2008) 104 [arXiv:0810.0714 [hep-ph]].

[45] M. Pospelov and A. Ritz, Phys. Lett. B **671**, 391 (2009) [arXiv:0810.1502 [hep-ph]].

[46] M. Pospelov, Phys. Rev. D **80**, 095002 (2009) [arXiv:0811.1030 [hep-ph]].

[47] M. Baumgart, C. Cheung, J. T. Ruderman, L. T. Wang, and I. Yavin, J. High Energy Phys. 04 (2009) 014 [arXiv:0901.0283 [hep-ph]].

[48] C. Cheung, J. T. Ruderman, L. T. Wang, and I. Yavin, Phys. Rev. D **80**, 035008 (2009) [arXiv:0902.3246 [hep-ph]].

[49] B. Batell, M. Pospelov and A. Ritz, Phys. Rev. D **79**, 115008 (2009) [arXiv:0903.0363 [hep-ph]].

[50] R. Essig, P. Schuster and N. Toro, Phys. Rev. D **80**, 015003 (2009) [arXiv:0903.3941 [hep-ph]].

[51] A. Hook, E. Izaguirre and J. G. Wacker, Adv. High Energy Phys. **2011**, 859762 (2011) [arXiv:1006.0973 [hep-ph]].

[52] T. Behnke, J. E. Brau, P. N. Burrows, J. Fuster, M. Peskin, M. Stanitzki, Y. Sugimoto, and S. Yamada *et al.*, arXiv:1306.6329 [physics.ins-det].

[53] M. Baak *et al.* (Gfitter Group Collaboration), Eur. Phys. J. C **74**, 3046 (2014) [arXiv:1407.3792 [hep-ph]].

[54] I. Hoenig, G. Samach, and D. Tucker-Smith, Phys. Rev. D **90**, 075016 (2014) [arXiv:1408.1075 [hep-ph]].

[55] S. Chatrchyan *et al.* (CMS Collaboration), J. High Energy Phys. 12 (2013) 030 [arXiv:1310.7291 [hep-ex]].

[56] J. M. Cline, G. Dupuis, Z. Liu, and W. Xue, J. High Energy Phys. 08 (2014) 131 [arXiv:1405.7691 [hep-ph]].

[57] (ATLAS Collaboration), ATLAS-CONF-2013-017, ATLAS-COM-CONF-2013-010.

[58] J. Alwall, M. Herquet, F. Maltoni, O. Mattelaer, and T. Stelzer, *MadGraph 5 : Going Beyond*, J. High Energy Phys. 06 (2011) 128 [arXiv:1106.0522], http://arxiv.org/abs/1106.0522.

[59] R. Aaij *et al.* (LHCb Collaboration), J. High Energy Phys. 04 (2014) 114 [arXiv:1402.2554 [hep-ex]].

[60] R. Aaij *et al.* (LHCb Collaboration), J. High Energy Phys. 08 (2013) 117 [arXiv:1306.3663 [hep-ex]].

[61] M. Karliner and J. L. Rosner, Phys. Rev. D **91**, 014014 (2015) [arXiv:1410.7729 [hep-ph]].

[62] B. Aubert *et al.* (BaBar Collaboration), Phys. Rev. Lett. **90**, 242001 (2003) [hep-ex/0304021].

[63] D. Besson *et al.* (CLEO Collaboration), Phys. Rev. D **68**, 032002 (2003) [Erratum-ibid. D **75**, 119908 (2007)] [hep-ex/0305100].

[64] K. Abe *et al.* (Belle Collaboration), Phys. Rev. Lett. **92**, 012002 (2004) [hep-ex/0307052].

[65] M. Karliner and J. L. Rosner, Phys. Rev. D **90**, 094007 (2014) [arXiv:1408.5877 [hep-ph]].

[66] W. A. Bardeen, E. J. Eichten, and C. T. Hill, Phys. Rev. D **68**, 054024 (2003) [hep-ph/0305049].

[67] M. A. Nowak, M. Rho, and I. Zahed, Acta Phys. Polon. B **35** (2004) 2377 [hep-ph/0307102].

[68] A. D. Martin, W. J. Stirling, R. S. Thorne, and G. Watt, Eur. Phys. J. C **63**, 189 (2009) [arXiv:0901.0002 [hep-ph]].

[69] C. Quigg, arXiv:0908.3660 [hep-ph].

[70] G. Altarelli and G. Parisi, Nucl. Phys. B **126**, 298 (1977).

[71] J. Butterworth, G. Dissertori, S. Dittmaier, D. de Florian, N. Glover, et al., *Les Houches 2013: Physics at TeV Colliders: Standard Model Working Group Report*, arXiv:1405.1067, http://arxiv.org/abs/1405.1067.

[72] J. Gao, M. Guzzi, J. Huston, H.-L. Lai, Z. Li, et al., *CT10 next-to-next-to-leading order global analysis of QCD*, *Phys.Rev.* **D89** (2014), no. 3 033009, arXiv:1302.6246, http://arxiv.org/abs/1302.6246

[73] R. D. Ball, V. Bertone, S. Carrazza, C. S. Deans, L. Del Debbio, et al., *Parton distributions with LHC data*, *Nucl.Phys.* **B867** (2013) 244–289, arXiv:1207.1303, http://arxiv.org/abs/1207.1303.

[74] F. Campanario, H. Czyż, J. Gluza, M. Gunia, T. Riemann, G. Rodrigo, and V. Yundin, J. High Energy Phys. 02 (2014) 114 [arXiv:1312.3610 [hep-ph]].